J Mater Sci: Mater Med (2009) 20:2091–2103
DOI 10.1007/s10856-009-3779-0

# Interfacial properties and in vitro cytotoxic effects of surface-modified near infrared absorbing Au-$Au_2S$ nanoparticles

**Mei Chee Tan · Jackie Y. Ying · Gan Moog Chow**

Received: 9 February 2009 / Accepted: 5 May 2009 / Published online: 26 May 2009


**Abstract** Near infrared (NIR) absorbing Au-$Au_2S$ nanoparticles were modified with surfactants of different hydrocarbon chain lengths to allow loading of anticancer drug, cisplatin. The interfacial interactions and surfactant chain length effects on drug loading, optical properties and cytotoxicity were discussed in this work. Short-chain surfactants were oriented closer to the surface normal and were adsorbed at higher densities. Surface modification also changed the optical properties of the particles. Notably, particles modified with short-chain surfactants exhibited a red shift, whereas particles modified with long-chain surfactants showed a blue shift. The in vitro cytotoxicity of drug-loaded surface-modified particles was dependent on the surfactants' chain length. Significant cytotoxicity was observed for 1 mg/ml of drug-loaded particles using surfactants with the shortest chain length. After NIR triggered drug release, the released Pt compounds were observed to be cytotoxic, while remaining nanoparticles did not exhibit any cytotoxicity. Also, the released Pt compounds upon NIR irradiation of drug-loaded particles were observed to be more toxic and had a different molecular structure from cisplatin.

**Electronic supplementary material** The online version of this article (doi:10.1007/s10856-009-3779-0) contains supplementary material, which is available to authorized users.

M. C. Tan · J. Y. Ying · G. M. Chow
Molecular Engineering of Biological and Chemical Systems, Singapore-MIT Alliance, 4 Engineering Drive 3, Singapore 117576, Singapore

M. C. Tan
e-mail: meichee.tan@gmail.com

J. Y. Ying
e-mail: jyying@ibn.a-star.edu.sg

J. Y. Ying
Department of Chemical Engineering, Massachusetts Institute of Technology, Cambridge, MA 02139-4307, USA

J. Y. Ying
Institute of Bioengineering and Nanotechnology, 31 Biopolis Way, The Nanos, Singapore 138669, Singapore

G. M. Chow (✉)
Department of Materials Science and Engineering, National University of Singapore, 9 Engineering Drive 1, Singapore 117576, Singapore
e-mail: msecgm@nus.edu.sg

## 1 Introduction

The deep tissue penetrating property of near infrared (NIR) and the reduced autofluorescence of tissues in the NIR region [1, 2] have driven the interest in NIR-absorbing nanoparticles for biomedical applications [3–8]. Our recent work [9, 10] had incorporated NIR light [1, 2] and NIR-absorbing nanoparticles [11–14] to develop a NIR-activated drug delivery system. Besides its tissue penetrating properties, NIR light makes a suitable choice as a drug release trigger since it does not have any cytotoxic effect on cells [15–17]. Non-toxic drug-loaded NIR-absorbing nanoparticles could be introduced systemically, where toxic drugs would be released only upon NIR exposure at the desired site. After drug release, the remaining NIR-absorbing nanoparticles should remain non-toxic. Thus, the NIR-activated drug release system would potentially reduce the adverse side effects of cancer chemotherapy, and allow for minimally invasive treatment of surgically inoperable tumors. The NIR-absorbing nanoparticles were composites of crystalline Au and amorphous $Au_xS$ (where $x \sim 2$) that exhibited absorption bands at $\sim$530 nm and 650–1100 nm in the NIR region [13, 14].

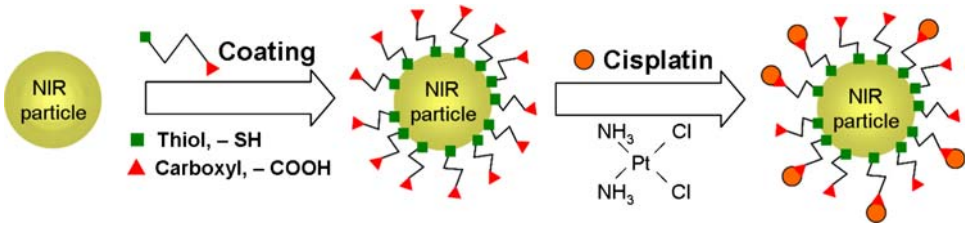


**Fig. 1** Schematic of NIR-activated Au-$Au_2S$ drug delivery system

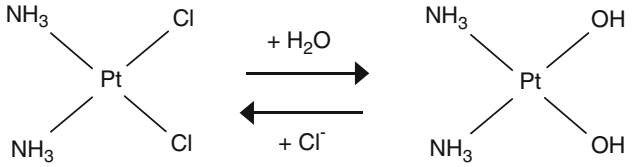


**Fig. 2** Structure of cisplatin in aqueous solutions

Surface characteristics of nanoparticles were tailored with surfactants to reduce the agglomeration tendency and enhance stability [18–20]. In addition, functionalization of NIR-absorbing nanoparticles with surfactants facilitated binding of the anticancer drug, cisplatin (Fig. 1) [9, 10]. The surfactants possessed thiol (–SH) and carboxyl (–COO) groups, which are reactive to NIR-absorbing nanoparticles and cisplatin, respectively [18, 21]. With labile Cl groups, cisplatin is hydroxylated in aqueous solutions (Fig. 2).

Surface chemistry of particles governed the binding and orientation of surfactants [21, 22]. While surfactant binding and orientation on films were addressed [18, 23, 24], the curvature effects of nanoparticles have remained unclear. Considering the higher curvatures of nanoparticles compared to films, surface energy of particles would be higher than that of films. Thus, surfactants would probably tilt closer towards particles' surfaces to reduce its surface energy. Furthermore, the tendency for surface segregation in multicomponent nanoparticles would change the surface composition and chemistry [25, 26].

In this work, mercaptoacetic acid (MAA), mercaptopropionic acid (MPA) and mercaptoundecanoic acid (MUA) were used to modify the NIR-absorbing nanoparticles. MAA, MPA and MUA have the same number of functional groups, and differed only by the hydrocarbon chain lengths. The difference in surfactant wetting properties with varying chain lengths modified surfactant orientation on particle surfaces [22]. Surfactants that tilt closer to the particle surface would impede the accessibility of binding sites, leading to reduced surfactant packing density. Thus, surfactants with different chain lengths were used to regulate drug loading. In addition, nanoparticle-surfactant interfacial interactions were used to manipulate the optical properties of NIR-absorbing particles.

With the increasing dominance of size and surface effects at the nanoscale, toxicity assessments of conventional bulk materials [27] and microparticles [28] may not be applicable to nanoparticles. Considering that in vivo clearance of non-biodegradable inorganic nanoparticles remained unclear, their significant accumulation within the systemic circulation was highly possible [29]. Recent studies on the in vitro carcinogenic effects and in vivo biodistribution of drug-loaded MUA-modified Au-$Au_2S$ were reported elsewhere [30, 31]. In this paper, the in vitro cytotoxicity of the Au-$Au_2S$ NIR-activated drug delivery system modified with different surfactants, on a commonly used breast cancer cell line, MCF-7 was assessed as a preliminary safety criterion. The cytotoxicity would probably be governed by the surface characteristics of particles, which would change nanoparticle-cellular interactions [32–35]. In addition, the adsorption of cisplatin onto surface-modified NIR-absorbing nanoparticles or the NIR irradiation might alter the structure of cisplatin or create new Pt complexes. Thus, upon NIR irradiation, the released Pt complexes could have different cytotoxic effects compared with native cisplatin.

## 2 Methods

### 2.1 Synthesis of NIR-absorbing nanoparticles

NIR-absorbing nanoparticles were synthesized by the reduction of aqueous $HAuCl_4$ (Sigma Aldrich) using aqueous $Na_2S$ (Sigma Aldrich) in a one-step mixing process [9, 10, 13, 14]. 1 mM of $Na_2S$ aged for 24 h was mixed with 2 mM of $HAuCl_4$ at S:Au precursor molar ratios of 0.6–0.8. Aging of $Na_2S$ was necessary due to the limited solubility of metal sulfides in water [36]. In this work, stirrer speed and reaction volume were fixed to achieve a consistent degree of mixing and diffusion rates. It was found that the as-synthesized NIR-absorbing nanoparticles were composites of amorphous $Au_xS$ (where $x \sim 2$) mixed with Au crystallites [13, 14].

### 2.2 Surface modification and drug loading

Mercaptoacetic acid (MAA, $HSCH_2COOH$), mercaptopropionic acid (MPA, $HS(CH_2)_2COOH$) and mercaptoundecanoic acid (MUA, $HS(CH_2)_{10}COOH$) were purchased

from Sigma Aldrich. Upon completing the synthesis of NIR-absorbing particles, water-soluble MAA and MPA were added directly into the reaction mixture at 100 mM. The insolubility of MUA in water required the chemisorption of MUA to be completed in absolute ethanol. NIR-absorbing particles were separated from the aqueous reaction mixture by centrifugation, and dispersed in 100 mM of MUA in absolute ethanol. The particles were dispersed in these surfactant-containing solutions for 3 days to allow surfactant chemisorption to reach equilibrium. Excess surfactants were removed by centrifugation. After $\geq$3 washes, the surfactant-coated nanoparticles were dispersed in 1 mg/ml of aqueous cisplatin (Sigma Aldrich). The adsorption of cisplatin took place over 2 days to ensure drug loading reached saturation. Excess cisplatin was removed by centrifugation, and drug-loaded colloids were washed at least three times with water before being redispersed in water.

## 2.3 NIR-activated drug release

Samples were irradiated at $\lambda = 1064$ nm using a Continuum® Minilite™ II Nd:YAG pulse laser operating with 50 mJ of pulse energy and 7 ns of pulse duration at 15 Hz. The focused beam size was $\sim$3 mm in diameter from burn paper measurements. A polarizing cube beamsplitter and a quarter waveplate were combined for use as an isolater to reject possible back reflections. The beam was directed using mirrors, and introduced from the liquid surface to minimize lensing effects that could arise from the sides of the vials.

## 2.4 Characterization

The UV–Visible spectra of NIR-absorbing nanoparticles were obtained with a resolution of 0.5 nm, using the Shimadzu UV1601 spectrophotometer equipped with a 2-nm band pass filter. Transmission electron microscopy (TEM) images of samples on 400-mesh carbon-coated copper grids were taken using the JEOL 3010 transmission electron microscope equipped with a $LaB_6$ gun operating at an accelerating voltage of 300 kV.

### *2.4.1 Qualitative chemical analysis of surface-modified particles*

Photoacoustic Fourier-transform infrared (PA-FTIR) spectra of freeze–dried samples purged with He was collected using the MTEC-200 photoacoustic cell and Biorad FTS-60A/896 spectrometer. The spectra were obtained at a speed of 5 kHz for with a resolution of 4 $cm^{-1}$.

### *2.4.2 Thermal analysis*

Thermal analysis of surface-modified particles was performed to estimate the amount of adsorbed surfactants and decomposition temperature. Thermal gravimetric analysis (TGA) was conducted in He using a Perkin–Elmer series 7 Thermal Analysis system with a ramp rate of 4°C/min. Freeze–dried samples were purged in He at room temperature for 30 min at the start to remove any free surface moisture. Weight gain from buoyancy effects were corrected by using the base line created from a repeated run of remaining samples upon completion of surfactant decomposition.

### *2.4.3 Stability of surface-modified nanoparticles*

Zeta potential was calculated using the Helmholtz–Smoluchowski equation [22]. Zeta potential measurements of particles dispersed in 0.1 M of sodium phosphate ($NaPO_4$) buffers were obtained using Malvern Instruments Zetasizer 2000. The pH was adjusted using 0.1 M of HCl and 0.1 M of NaOH to keep the ionic strength of different solutions constant. The zeta potential data presented represented the average taken from 5 measurements.

Dynamic light scattering (DLS) measurements of particles dispersed in 0.1 M of $NaPO_4$ buffers were taken using Brookhaven Instruments ZetaPlus systems. The diffusion coefficients were converted to hydrodynamic diameters using the Stokes-Einstein equation, and intensity-averaged size distributions were converted to number-averaged size distributions for further analysis. The hydrodynamic diameter data presented here represented the average of 5 measurements.

### *2.4.4 Adsorption and release of cisplatin*

Cisplatin loading on particles was estimated by chemical microanalysis on 200-mesh carbon-coated copper grids with the VG HB603 scanning transmission electron microscope (STEM) operating at 250 kV, equipped with a field emission gun and wide-angle X-ray detector. The characteristic Pt and Au peak areas were normalized with respect to the Cu peak area to estimate the Pt and Au concentrations at the surfaces and cores of five different particles.

Cisplatin adsorption was further verified by measuring the cisplatin concentration in the supernatant after drug loading. The cisplatin concentration in aqueous solutions was measured at 210 nm using the Waters high-performance liquid chromatography (HPLC) Alliance system equipped with a UV–visible detector, and Betasil-C18 column (250 mm $\times$ 4.6 mm I.D.) packed with 5-μm particles. Isocratic conditions were used with 90:10 v/v of acetonitrile:water and a flow rate of 1 ml/min.

#### 2.4.5 Molecular structure of released compounds in supernatant fraction

Mass spectrometry (MS) analysis was performed using Applied Biosystems API 2000 LC/MS/MS system with atmospheric pressure chemical ionization, operating in the flow injection analysis mode. Water with 0.1% formic acid was used as the carrier solvent with a flow rate of 0.2 ml/min.

$^1$H nuclear magnetic resonance (NMR) spectra of the released compounds were obtained in 5 v/v% $D_2O$ over ~12 h using a Bruker Avance II spectrometer equipped with a 400 MHz Ultrashield magnet. Chemical shifts were recorded as parts per million (ppm) relative to tetramethylsilane.

#### 2.4.6 In vitro cytotoxicity assay

Adherent human breast adenocarcinoma cells, MCF-7 (American Type Culture Collection (ATCC)) were cultured in a 75-cm$^2$ tissue culture flask using Eagle's Minimum Essential Medium (EMEM) supplemented with 10 v/v% fetal bovine serum (FBS) and 0.01 mg/ml of insulin, and incubated at 37°C in a humidified atmosphere with 5 v/v% $CO_2$. Upon reaching 80% confluence, MCF-7 cells were harvested for in vitro cytotoxicity tests, using the 3-[4,5-dimethylthiazol-2-yl]-2,5-diphenyl-tetrazolium bromide (MTT) toxicology assay. Mitochondrial dehydrogenases from metabolically active cells reduced MTT to yield water-insoluble purple formazan crystals that were soluble in acidified isopropanol. Cell viability and proliferation rates obtained using spectrophotometric quantification of formazan crystals would be indicative of the degree of cytotoxicity induced by test materials.

Each test sample was repeated at least 12–18 times to yield statistically representative data. In addition, each test included a similar number of blanks containing only serum-free media to form the basis for normalizing the data collected. Approximately $20 \times 10^3$ to $40 \times 10^3$ cells suspended in culture media were seeded in each well. After ~12 h of incubation to allow adhesion of cells to the base of wells, the culture medium was removed and discarded. The cells were rinsed once with phosphate buffer saline (PBS) solution. Subsequently, 100 µl of nanoparticles at different concentrations dispersed in serum-free EMEM were introduced, and incubated with the cells for 24 h. The nanoparticles were then removed and discarded. Cells were rinsed with PBS before 100 µl of serum-free EMEM media were added to each well, followed by 10 µl of MTT in PBS (5 mg/ml). They were incubated for another ~3 h for the precipitation of MTT formazan crystals. MTT formazan crystals were dissolved, and the cell viability was determined from solution absorbance at 570 nm measured using the Biorad Model 680 microplate reader.

## 3 Results and discussions

### 3.1 Surface modification and stability of NIR-absorbing nanoparticles

#### 3.1.1 Adsorption of surfactants from FTIR spectra

The FTIR spectra in Fig. 3 for MAA-, MPA- and MUA-modified particles displayed the characteristic chemical groups of the respective surfactants (see Supporting Information (SI)) [37]. The variations in peak positions for similar chemical groups between MAA- and MPA-modified particles and MUA-modified particles indicated differences in surfactant orientation and interfacial interactions that depended on the surfactant chain length. The broad band for MAA-modified particles at ~3420 cm$^{-1}$ were assigned to the OH stretching mode of water [38]. Interactions with water were more favorable for surfactants with short hydrocarbon chains (e.g. MAA), compared to long-chain surfactants (i.e. MUA).

#### 3.1.2 Thermal stability of surfactants on NIR-absorbing nanoparticles

From thermal desorption mass spectroscopy of surfactants from film substrates, thermal stability of surfactants was reported to increase with increased hydrocarbon chain length with a dependence on surface coverage [39]. Using an identical approach, thermal stability of surface-modified NIR-absorbing nanoparticles was evaluated.

More short-chain surfactants were adsorbed on the particles (Table 1). This suggested that short-chain surfactants had its C–C axis oriented away from particle surface (see Fig. 4); this would expose more binding sites leading to increased surfactant adsorption. Thus, short-chain surfactants were packed at a higher density on the

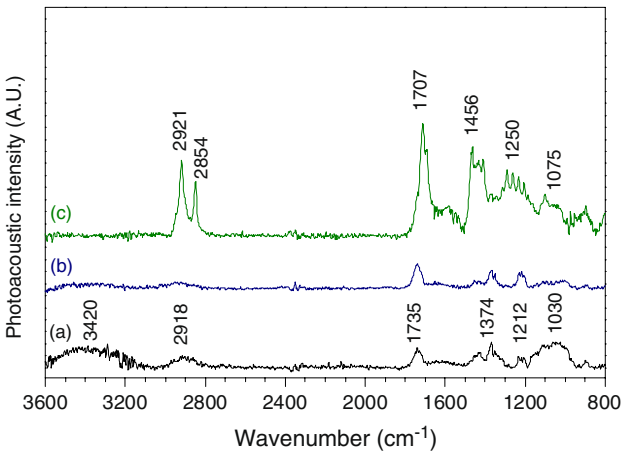


**Fig. 3** FTIR spectra of (a) MAA-modified, (b) MPA-modified and (c) MUA-modified NIR-absorbing nanoparticles

particle surface. Considering that long-chain surfactants were oriented closer to the surface, surface energy of particles was further reduced to enhanced particle stability.

Particles modified with short-chain surfactants, MAA and MPA, had a lower decomposition temperature than those modified with long-chain surfactant, MUA. The higher decomposition temperature for MUA-modified particles suggested increased entanglement between MUA chains and increased interactions between MUA and particle surface. Since the amount of adsorbed long-chain surfactant MUA was less than short-chain surfactants MAA and MPA, the increased interactions between MUA and particles further showed that MUA was oriented closer to the surface than MAA and MPA. The higher decomposition temperature and interfacial interactions of MUA indicated that MUA-modified particles were more stable with a lower surface energy than MAA- and MPA-modified particles.

### 3.1.3 *Thickness of surfactant layer estimated from TEM micrographs*

Considering the particle surface area ($4\pi r^2$) and projected area occupied by a S atom ($\pi r^2$), the estimated maximum possible amount of adsorbed surfactants was $\sim 156 \times 10^4$ atoms/particle for a monolayer. From the measured adsorbed surfactants amount (Table 1), the estimated number of adsorbed surfactants was $\sim 113 \times 10^3$ atoms/particle for MAA- and MPA-modified particles, and $\sim 75 \times 10^3$ atoms/particle for MUA-modified particles. Since the measured estimates of adsorbed surfactants were significantly less than the estimated maximum possible in a monolayer, this indicated that no more than a single layer of surfactants was coated on the nanoparticles.

Figure 5 shows a $\sim$5-nm coating of MUA surfactants around a typical nanoparticle. TEM observations of MAA- and MPA-modified particles were hindered by rapid ablation of surfactants by the incident electron beam due to their lower decomposition temperature (Table 1). However, estimates made during TEM operation suggested that the thickness of MAA and MPA coating was $\ll$1 nm. Coating thickness for surfactant-modified particles was also deduced from the DLS hydrodynamic diameter (see SI). Coating thickness for short-chain surfactants MAA and MPA was $\sim$1–2 nm, while coating thickness of long-chain surfactant MUA was $\sim$5–6 nm. The latter was consistent with that determined from TEM observations.

### 3.1.4 *Stability of surface-modified NIR-absorbing nanoparticles in $NaPO_4$ buffer*

Zeta potential for MUA-modified particles from Fig. 6 showed little difference in isoelectric point between the modified and the uncoated colloids. This was due to the minor difference between the isoelectric point of uncoated particles (pH $\sim$ 5) and the calculated pKa estimate of MUA ($\sim$4.78 $\pm$ 0.20) [40]. However, MUA-modified

**Table 1** Thermal analysis of surface-modified NIR-absorbing nanoparticles

| | Average adsorbed (μmol/mg) | Decomposition temperature (°C) |
|---|---|---|
| MAA-modified | 0.14 ± 0.01 | ~150 |
| MPA-modified | 0.16 ± 0.01 | ~150 |
| MUA-modified | 0.10 ± 0.03 | ~200 |

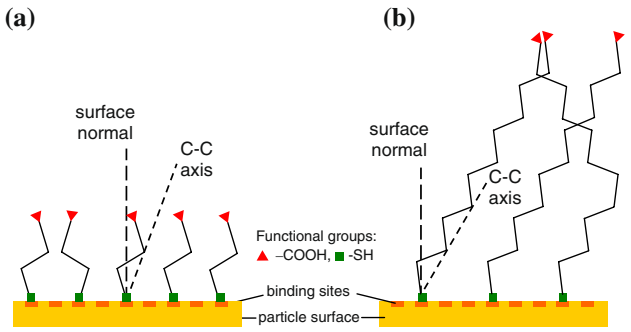


**Fig. 4** Schematic representation of interfacial interactions between particle surfaces and **a** short-chain and **b** long-chain surfactants

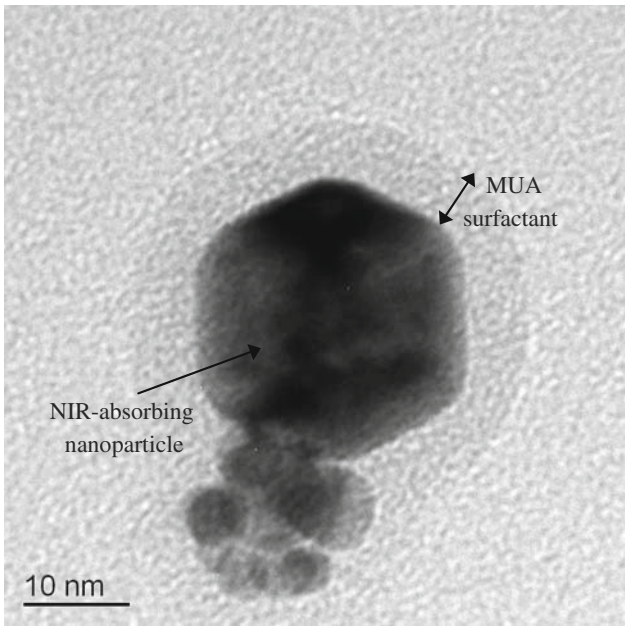


**Fig. 5** TEM micrograph of MUA-modified nanoparticles

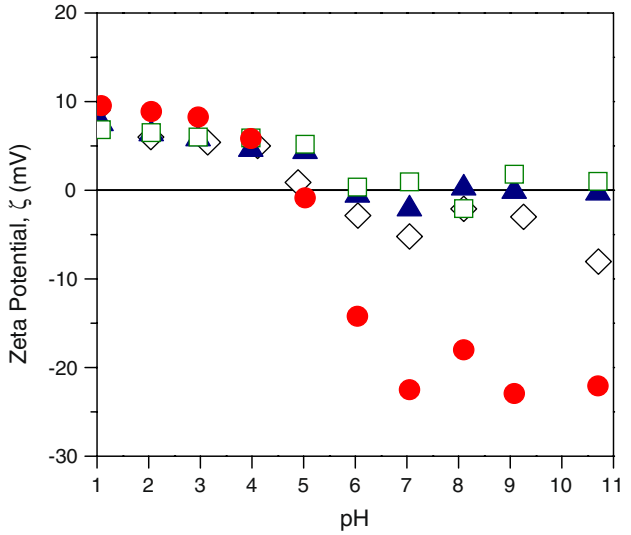


**Fig. 6** Zeta potential of (◇) uncoated, (▲) MAA-modified, (□) MPA-modified and (●) MUA-modified NIR-absorbing nanoparticles

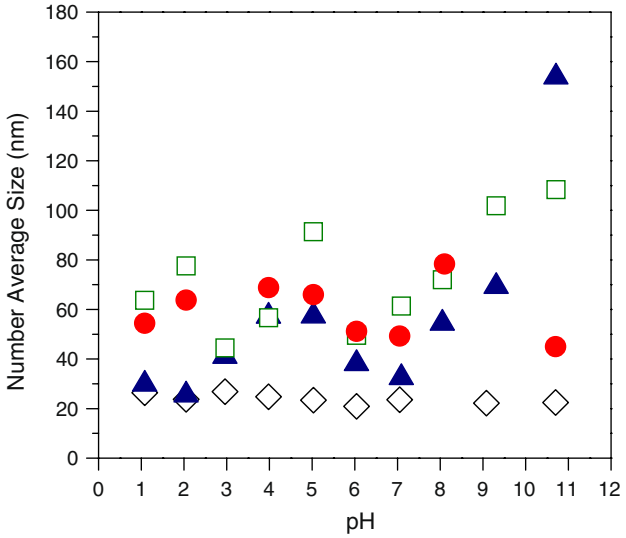


**Fig. 7** DLS particle size distributions of (◇) uncoated, (▲) MAA-modified, (□) MPA-modified and (●) MUA-modified NIR-absorbing nanoparticles

particles had a higher surface charge (∼20 mV) than uncoated particles (∼7 mV) for pH 6–10. The higher negative surface charge was attributed to the deprotonation of carboxylic acid groups ($COOH \rightarrow COO^-$) on the surfactants.

For MAA- and MPA-modified particles, there was no distinct isoelectric point (Fig. 6), and the measured zeta potential fluctuated about zero for pH 6–10. This was due to the formation of flocs induced by interactions between $COO^-$ on surfactants and $Na^+$ ions within the $NaPO_4$ buffer. The change in effective hydrodynamic diameters indicated flocculation for MAA- and MPA-modified particles (Fig. 7). In contrast, uncoated and MUA-modified particles had relatively constant diameters and showed no signs of flocculation. It should be noted that data were taken ∼30 min after dispersion of colloids in buffer since flocculation was a reversible and dynamic process.

The difference in particle stability using surfactants of different chain lengths was attributed to the difference in particle separation distances. In the absence of electrostatic stabilization, stability of MAA- and MPA-modified particles was governed by steric stabilization only. With their shorter interparticle separation distance (i.e. coating thickness ∼1–2 nm), steric stabilization of short-chain surfactant modified particles was insufficient to prevent flocculation. In contrast, the increased entanglement of MUA chains would have probably prevented neutralization of $COO^-$ from $Na^+$. With both electrostatic and steric stabilization, flocculation of MUA-modified particles was prevented. The enhanced stability of MUA-modified particles verified the earlier deduction of MUA-modified particles having a lower surface energy.

### 3.2 Effect of surfactant chain length on optical properties

MAA- and MPA-modified nanoparticles showed a red shift and broadening of absorption bands (see SI). In contrast, MUA-modified nanoparticles showed a blue shift and a similar broadening of absorption bands (see SI). Upon coating the particles with surfactants, electron scattering increased as absolute surface area increased. This led to increased damping of plasma oscillations and resulted in the broadening of absorption bands [41]. It was reported that adsorption of small amounts of $SH^-$ caused a blue shift in the absorption band of Ag, while adsorption of $SH^-$ at larger amounts led to a red shift [42]. The effects of different adsorbate concentrations on Ag absorption band positions were not established in the reported work [42]. However, consistent with these reported effects, adsorption of short-chain surfactants MAA and MPA in larger amounts had resulted in a red shift, while adsorption of long-chain surfactants MUA in smaller amounts had resulted in a blue shift (Fig. 8).

Inhomogeneous surface polarization of large Au nanoparticles (>25 nm) with increasing size led to higher order of plasma oscillations that resonated at lower frequencies [41, 43]. This resulted in the red shift of plasmon absorption band with increasing particle size. Considering that absorption band of larger MUA-modified particles (58 ± 9 nm) showed a blue shift in contrast to the red shift shown by smaller MAA- and MPA-modified particles (50 ± 4 nm), size effects would not account for the observed shift. The shift in absorption band was thus attributed to difference in the surface characteristics of

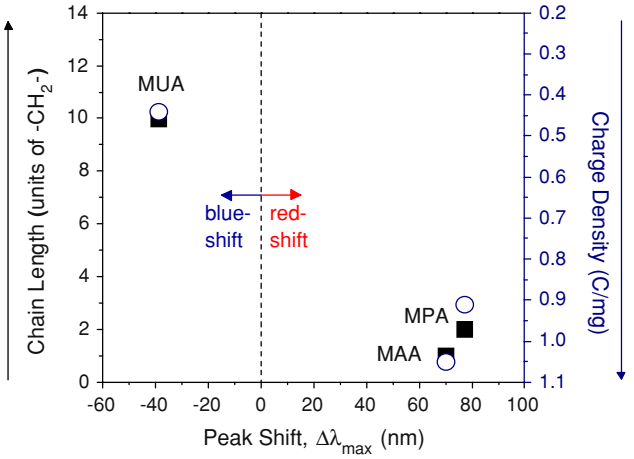


**Fig. 8** Relationships between surfactant (■) chain length and (○) charge density and the absorption peak position of nanoparticles

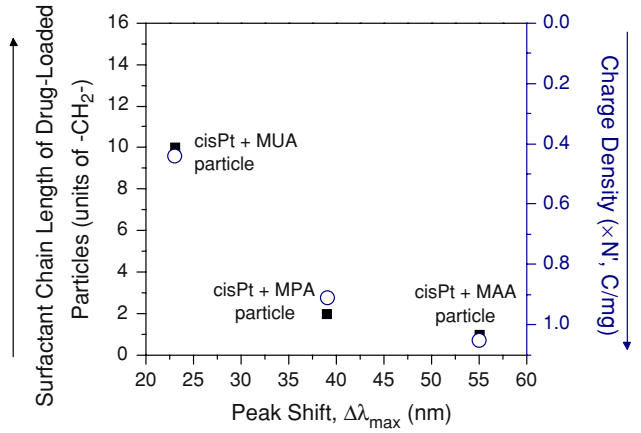


**Fig. 9** Relationships between surfactant (■) chain length and (○) charge density and the absorption peak position of drug-loaded nanoparticles

particles. The surface modification of particles had altered the surface polarizability to result in shift in plasmon resonance frequencies.

If one considers that each surfactant had one free electron upon deprotonation of its carboxyl group, the electronic charge available for each surfactant would be $\sim 1.602 \times 10^{-19}$ C/molecule. Surface charge density for surface-modified particles was thus deduced from the electronic charge per surfactant and the adsorbed surfactant amount in Table 1. MAA- and MPA-modified particles were estimated to have a higher surface charge density than MUA-modified particles. The absorption band was found to blue-shift at low surface charge density and red-shift at higher surface charge densities (see Fig. 8). The difference in surface charge density (~25 times) altered the surface polarizability of particles to modify plasmon resonating frequencies. Subsequently, absorption bands were shifted in different directions. However, the exact relationship of surface effects and surface charge density to plasmon resonating frequencies remained unclear.

Cisplatin adsorption on the surface-modified particles resulted only in red shifts (SI). Cisplatin adsorption on MUA-modified particles resulted in less red shift than that on MAA- and MPA-modified particles (Fig. 9). The exact number of free electrons contributed by adsorbed cisplatin remained unknown. However, considering a monolayer of drug adsorption where cisplatin contributed N′ electrons, the surface charge density for drug-loaded particles would decrease with increasing surfactant chain lengths. The subsequent change in surface polarizability of particles modified the plasmon resonating frequencies. The trend of decreasing red shift with decreasing charge density in Fig. 9 was consistent with that in Fig. 8. In addition, as the surface area increased further upon cisplatin adsorption, increased electron scattering resulted in additional broadening of absorption bands [41].

### 3.3 Effect of surfactant chain length on drug loading and release

Table 2 shows that more cisplatin was loaded onto MAA- and MPA-modified particles than MUA-modified particles. This was attributed to the higher number of short-chain surfactants adsorbed on the particles (Table 1), which provided more drug binding sites. The ratio of short chain to long chain surfactants adsorbed on the particles was 1.5 (Table 1), which was quite consistent with the cisplatin loading ratio of 2.0 on particles modified with short-chain to long-chain surfactants (Table 2). This suggested that approximately a monolayer of cisplatin was adsorbed on the surface-modified particles.

Drug adsorption kinetics was evaluated by normalizing the adsorbed cisplatin concentration with the saturated adsorbed cisplatin concentration. The profiles in Fig. 10 were characteristic of Langmuir isotherms, which confirmed the monolayer adsorption of cisplatin. Long-chain surfactant modified particles showed slightly slower adsorption kinetics than short-chain surfactants modified particles (Fig. 10). This suggested that while drug loading was changed by using surfactants with different chain lengths, the chain length had little effects on adsorption kinetics. Further work on drug binding mechanisms would be warranted, which is beyond the scope of this work.

Drug release was triggered by exposure of drug-loaded particles to irradiation at $\lambda = 1064$ nm using a Nd:YAG pulse laser. It was estimated that ~80–90% of adsorbed cisplatin was released after ~1 h. This suggested that most drugs were chemisorbed onto the particles, and the leaching of drugs from the particles was negligible. Drug release profiles were evaluated after normalizing with the maximum amount released. Considering the rapid release kinetics (Fig. 11), no conclusions could be made on the

**Table 2** STEM EDX elemental analysis of drug-loaded NIR-absorbing nanoparticles. At least five different particles were analyzed for each sample

| Element | MAA-modified | | MPA-modified | | MUA-modified | |
|---|---|---|---|---|---|---|
| | Core | Surface | Core | Surface | Core | Surface |
| Au peak area | 86.6 | 72.9 | 119.9 | 84.9 | 190.9 | 155.1 |
| Pt peak area | – | 24.0 | 4.1 | 23.3 | – | 21.3 |
| Pt/Au surface conc. ratio | | 0.33 | | 0.27 | | 0.14 |

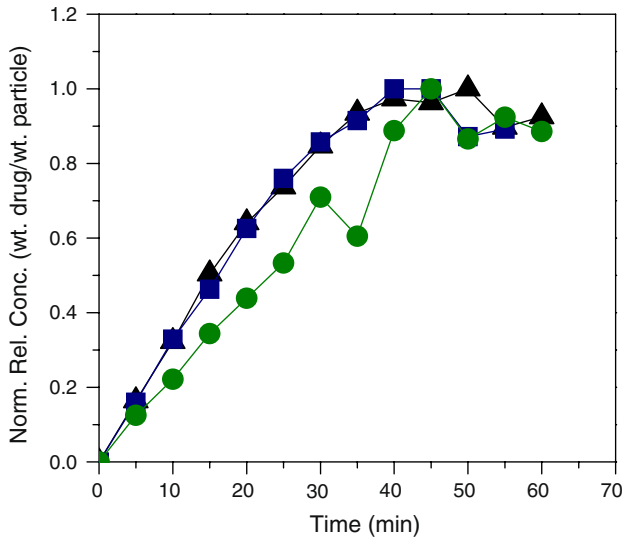


**Fig. 10** Drug absorption profiles on (▲) MAA-modified, (■) MPA-modified and (●) MUA-modified nanoparticles

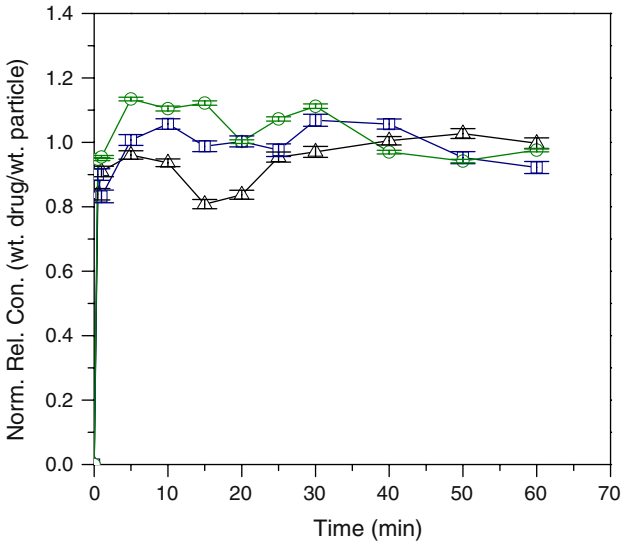


**Fig. 11** Drug release profiles from (△) MAA-modified, (□) MPA-modified and (○) MUA-modified nanoparticles using a pulse laser at $\lambda = 1064$ nm

dependence of drug release and strength of surfactant-drug interactions on surfactant chain length.

### 3.4 In vitro cytotoxicity of surface-modified particles

The in vitro cytotoxic effects induced by particles with different surface characteristics and drug loadings were evaluated. Considering that typical standard deviations were ~15%, cytotoxic effects were not statistically significant for normalized cell viability of 0.7–1.3, using a 95% confidence interval.

Nanoparticles modified using surfactants of different hydrocarbon chain lengths, and surfaces enriched with S after NIR irradiation [14], showed no cytotoxic effects (Fig. 12). No significant cytotoxic effects were observed for drug-loaded MPA-modified nanoparticles and drug-loaded MUA-modified nanoparticles before and after drug release (Fig. 13). However, 1 mg/ml of drug-loaded MAA-modified nanoparticles exhibited significant reduction in cell viability (Fig. 13). Upon NIR-activated drug release, the initial cytotoxic effects of drug-loaded MAA-modified nanoparticles were no longer observed.

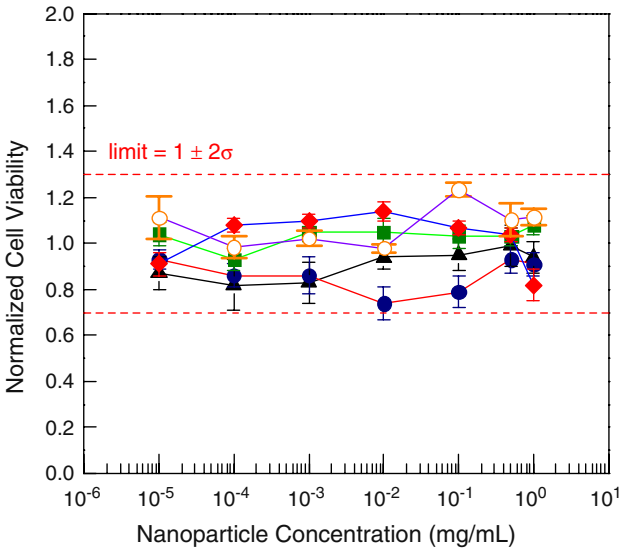


**Fig. 12** Cytotoxicity of (▲) unmodified nanoparticles before NIR irradiation, and (○) unmodified, (●) MAA-modified, (■) MPA-modified and (♦) MUA-modified nanoparticles after NIR irradiation

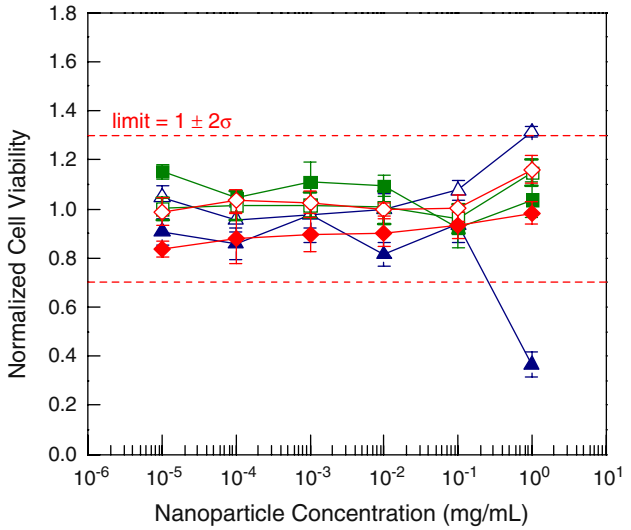


**Fig. 13** Cytotoxicity of drug-loaded (▲, Δ) MAA-modified, (■, □) MPA-modified and (♦, ◇) MUA-modified nanoparticles before (*close symbols*) and after drug release (*open symbols*)

Supernatant of drug-loaded particles incubated in growth media for 24 h was collected to verify the effects of drug leaching. Cytotoxic effects from drug leaching were insignificant, since no change in cell viability was observed (Fig. 14). The absence of drug leaching indicated that a stable chemical bond was formed between the drug and surfactants. Considering that both MAA-modified and MPA-modified nanoparticles had similar drug-loading, this indicated that cytotoxic effects of 1 mg/ml of drug-loaded MAA-modified nanoparticles were not triggered by interactions between surface-loaded drugs with cells only. The main cause for cytotoxicity related to 1 mg/ml of drug-loaded MAA-modified nanoparticles could not be established here. However, this suggested that the entire assembly, which included synergistic effects of nanoparticle-surfactant-drug interactions, would need to be considered to evaluate possible causes of cell death.

### 3.5 In vitro cytotoxicity of compounds released from particles

The in vitro cytotoxic effects from the supernatant fraction that contained released Pt compounds, collected after NIR irradiation of drug-loaded particles, were examined. The concentration of Pt compounds released was determined from the absorbance at 210 nm using HPLC. No changes in the peak distribution with respect to residence time for HPLC chromatographs of the released substances were observed. The unchanged chromatographs indicated that Pt compounds were released, since most Pt compounds including cisplatin would show absorption at 210 nm.

The released Pt compounds were more cytotoxic to MCF-7 than cisplatin (Fig. 15). This suggested that lower drug concentration and consequently lower particle dosage would be required to achieve similar toxicity. Increased toxicity of the supernatant fraction could have been caused by either synergistic effects of the released surfactants with cisplatin or the formation of other Pt compounds brought upon by structural changes on cisplatin. The toxicity exhibited by cisplatin was strongly influenced by its structure [44–46]. Pt compounds (e.g. carboplatin) formed by the coordination of Pt with other molecules have been noted to exhibit different toxic characteristics from cisplatin [44–46].

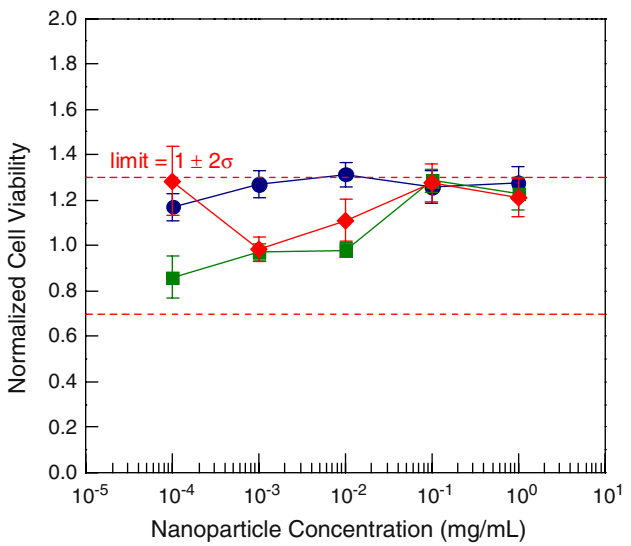


**Fig. 14** Cytotoxicity of the supernatant collected from drug-loaded (●) MAA-modified, (■) MPA-modified and (♦) MUA-modified nanoparticles

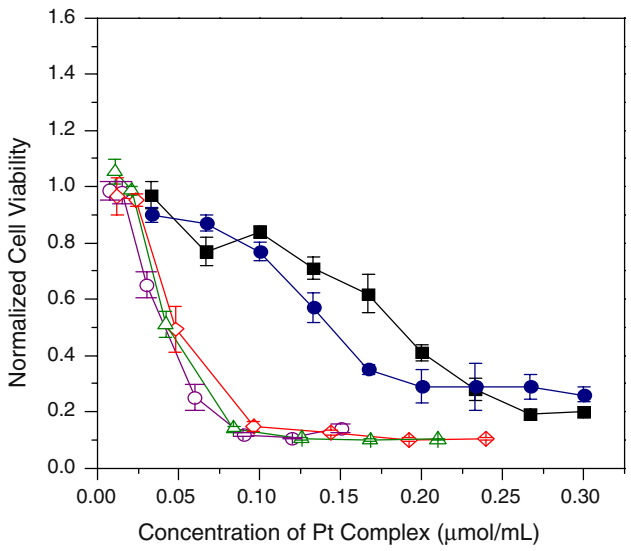


**Fig. 15** Cytotoxicity of native cisplatin (■) before and (●) after NIR irradiation, and "Pt compounds" released from (Δ) MAA-modified, (◇) MPA-modified and (○) MUA-modified nanoparticles

Surfactants alone did not give rise to cytotoxic effects (see SI). Cisplatin mixed with 0.15 μmol/ml of surfactants did not show different cytotoxicity from cisplatin (see SI). Therefore, there were no synergistic cytotoxic effects between cisplatin and surfactants. In addition, Fig. 15 illustrates that NIR irradiation of cisplatin alone did not change its cytotoxicity substantially. Thus, the increased cytotoxicity of the released Pt compounds in Fig. 15 compared to cisplatin was most likely a result of structural changes to cisplatin.

NMR and mass spectroscopies were used to elucidate the molecular structure of Pt compounds released upon NIR irradiation of the drug-loaded particles. $^{1}$H NMR spectra of cisplatin and Pt compounds released from modified particles were collected (see SI). The assignments of the NMR peaks for cisplatin are summarized in Table 3 [47]. The broad peak for cisplatin at ~3.9–4.2 ppm was attributed to the averaging effects on electronic motion from random molecular movements in aqueous cisplatin solution [38]. The peaks at ~1.15 ppm and 2.17 ppm corresponded to species that were less electronegative than Pt, such as $NH_4^+$ and $NH_4OH$, respectively, which were formed by $NH_3$ dissociation from cisplatin.

NMR spectra collected for the compounds released from surfactant-modified particles exhibited peaks at similar positions. Thus, if surfactants were released upon NIR irradiation of drug-loaded particles, the surfactants did not alter the electronic environment of the released compounds. The $^{1}$H NMR spectra of released compounds were different from that of cisplatin, suggesting that the released compounds had a different molecular structure from cisplatin. The increased intensity of the ~2.17 ppm peak for released compounds when compared to cisplatin indicated that $NH_3$ dissociation increased after NIR irradiation. The peak at ~4.7 ppm corresponded to the H nuclei of water [48], which was detected due to the low concentrations (~μmol/ml) of released compounds in the NMR test samples. The other peaks at ~1.2, 1.5, 2.6 and 3.2 ppm could not be assigned to a chemical group without the separation of the different fragments or using a suitable reference in similar physical and chemical environments.

The mass spectra of cisplatin and the supernatant collected after NIR irradiation of drug-loaded particles are presented in Figs. 16 and 17, respectively. The noise and broad peaks observed, particularly at 240–320 a.m.u., was attributed to different isotopes of elements in cisplatin, and differing degrees of H substitution in $NH_3$ and OH groups of cisplatin. Peaks observed from the mass spectra of cisplatin (Fig. 16) and released compounds (Fig. 17) were assigned based on previous reports [44–46], or appropriate combinations of elements (i.e. Pt, Cl, $NH_3$, OH, Au, COO, C, S) present in aqueous solutions (see SI).

The mass spectra for the released compounds in Fig. 17 were similar for drug-loaded particles modified with different surfactants. However, mass spectra of these released compounds were different from that of cisplatin. In particular, the peaks located at 223 a.m.u, 391 a.m.u and 413 a.m.u. were not exhibited by cisplatin. Additional complexes of $Pt(NH_3)_2(COO)$, PtAu or $PtAuC_2$, in the released compounds were observed in all the supernatants collected after NIR irradiation of drug-loaded MAA-, MPA- and MUA-modified particles (see Fig. 17). $Pt(NH_3)_2(COO)$ was most likely formed during the chemisorption of cisplatin onto surfactants. The complexes of Pt and Au (PtAu or $PtAuC_2$) were most likely formed by interactions between released cisplatin and melted Au from the particles during NIR irradiation [37]. While certain Pt and Au complexes were reported to exhibit toxic effects [44–46, 49, 50], toxicities of the proposed $Pt(NH_3)_2(COO)$, PtAu or $PtAuC_2$ complexes have not been reported. Since such complexes were the main difference between the supernatant fraction

**Table 3** Assigned $^{1}$H NMR peaks for cisplatin [47]

| $^{1}$H chemical shift, $\delta$ (ppm) | Assignment |
|---|---|
| 3.59 | $Pt(NH_3)_2(OH)_2$ |
| 3.60 | $Pt(NH_3)_2(OH)Cl$ |
| 3.98 | $Pt(NH_3)_2(OH)(H_2O)$ |
| 4.05 | $Pt(NH_3)_2(OH)Cl$ |
| 4.06 | $Pt(NH_3)_2(Cl)_2$ |
| 4.25 | $[Pt(NH_3)_2(H_2O)Cl]_2$ |
| 4.33 | $[Pt(NH_3)_2(H_2O)Cl]_2$ |
| 4.51 | $[Pt(NH_3)_2(H_2O)_2]_2$ |

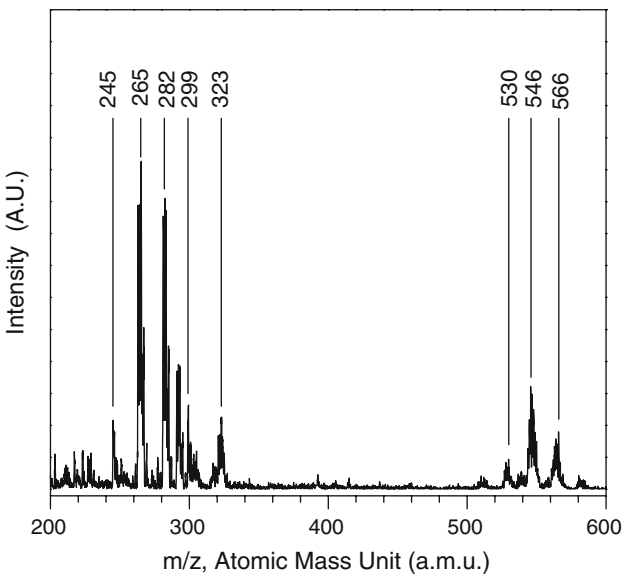


**Fig. 16** Mass spectrum of cisplatin

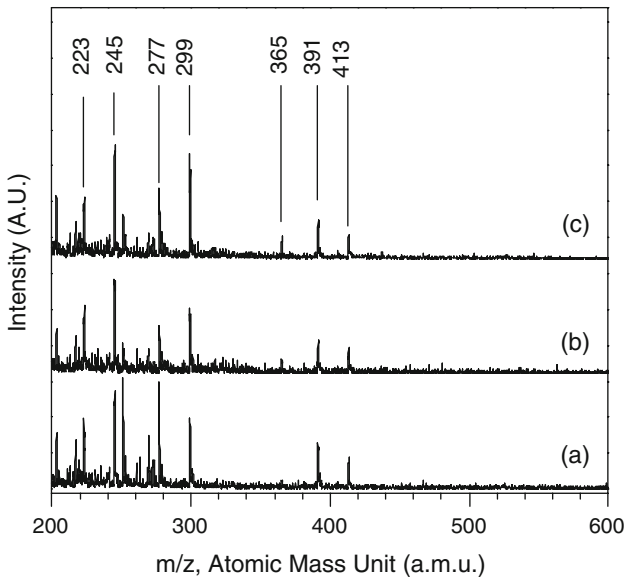


**Fig. 17** Mass spectra of "Pt compounds" released to the supernatant from (a) MAA-modified, (b) MPA-modified and (c) MUA-modified nanoparticles. The peaks at 277, 391 and 413 a.m.u. can be attributed to $Pt(NH_3)_2(COO)$, PtAu and $PtAuC_2$, respectively

and cisplatin, one or more of them would be the most likely cause(s) for the increased cytotoxicity of the collected supernatant (Fig. 15).

If complexes of Pt and Au were indeed the governing factor for increased cytotoxicity, it could relate to the cytotoxic effects for 1 mg/ml of drug-loaded MAA-modified particles, relative to that of drug-loaded MPA-modified nanoparticles and drug-loaded MUA-modified nanoparticles (Fig. 13). Since MAA separated cisplatin from Au particles with only one hydrocarbon, the close proximity between Au and Pt in this case was likely to have allowed toxic effects that resulted from either PtAu or $PtAuC_2$ complexes in becoming noticeable. This would be consistent with the earlier claim that the cytotoxic effects of this system were related to synergistic effects of drug-surfactant-nanoparticle interactions. In contrast, MPA and MUA separated cisplatin from Au particles with a greater distance (2 and 10 hydrocarbons, respectively), which would diminish the synergistic effects of drug-surfactant-nanoparticle interactions, if any. Thus, no cytotoxic effects were exhibited by drug-loaded MPA-modified and drug-loaded MUA-modified particles.

## 4 Conclusions

NIR-absorbing Au-$Au_2S$ nanoparticles were modified with surfactants of different chain lengths to allow surface loading of anticancer drug, cisplatin. Further system optimization (e.g. excitation source and particle absorption wavelengths) for actual clinical application would be required, which is beyond the scope of this work. In this work, interfacial interactions were characterized and surfactant chain length effects on drug loading, optical properties and cytotoxicity were studied. The difference in orientation due to surfactant hydrocarbon chain length resulted in higher packing densities of short-chain surfactants adsorbed on NIR-absorbing nanoparticles. Consequently, higher surface drug loading was achieved by using short-chain surfactant modified particles. In addition, surface modification of particles with surfactants and cisplatin resulted in the shifting of absorption bands along with considerable band broadening. Notably, particles modified with short-chain surfactants exhibited a red shift, whereas particles modified with long-chain surfactants showed a blue shift. The change in optical properties was attributed to altered surface polarizability from difference in surface charge density from surfactants. However, the exact relationship between the surface effects and the surface charge density to plasmon resonating frequencies remained unclear.

The in vitro cytotoxicity of NIR-activated drug delivery system on breast cancer cells MCF-7 was also examined. The results showed that the proposed NIR-absorbing drug delivery system would be generally regarded as safe for concentrations below 1 mg/ml. Both drug-loaded MPA-modified and drug-loaded MUA-modified nanoparticles exhibited no significant cytotoxic effects before and after the NIR triggered drug release. However, at a high concentration of drug-loaded MAA-modified nanoparticles (i.e. 1 mg/ml), a significant cytotoxicity was observed. Upon NIR triggered drug release, the remaining nanoparticles did not show any cytotoxic effects. Released Pt compounds from nanoparticles were more toxic to breast cancer cells than native cisplatin. Therefore, from the result of these cytotoxicity studies, considering that the drug-loaded particles were not toxic, side effects that would have otherwise been induced during chemotherapy from toxicity of cisplatin would be reduced. Upon NIR exposure at the tumor site, drugs would be released from the particles. For the NIR triggered drug delivery system to be effective, the released drugs should be toxic, while remaining particles remaining non-toxic. This work had shown that the released drugs were more toxic than cisplatin. This suggests that a lower particle dosage would be required to achieve similar lethality.

**Acknowledgements** This work was supported by the funding from the Singapore-MIT Alliance and NUS academic research grant. Gan Moog Chow thanks the support of Office of Naval Research, USA. The authors thank Binghai Liu for assistance in TEM, and Eric A. B. Kantchev, Jaehong Lim and Su Seong Lee of the Institute of Bioengineering and Nanotechnology for their assistance with the LC/MS/MS and NMR spectroscopies.

## References


1. Frangioni JV. In vivo near-infrared fluorescence imaging. Curr Opin Chem Biol. 2003;7:626–34. doi:10.1016/j.cbpa.2003.08.007.
2. Weissleder R. A clearer vision for in vivo imaging. Nat Biotechnol. 2001;19:316–7. doi:10.1038/86684.
3. Oldenburg SJ, Averitt RD, Westcott SL, Halas NJ. Nanoengineering of optical resonances. Chem Phys Lett. 1998;288:243–7. doi:10.1016/S0009-2614(98)00277-2.
4. Loo C, Lowery A, Halas N, West J, Drezek R. Immunotargeted nanoshells for integrated cancer imaging and therapy. Nano Lett. 2005;5:709–11. doi:10.1021/nl050127s.
5. Hirsch LR, et al. Nanoshell-mediated near-infrared thermal therapy of tumors under magnetic resonance guidance. Proc Natl Acad Sci USA. 2003;100:13549–54.
6. Sershen S, West J. Polymeric systems for modulated drug delivery. Adv Drug Deliv Rev. 2002;54:1225–35. doi:10.1016/S0169-409X(02)00090-X.
7. Hirsch LR, Jackson JB, Lee A, Halas NJ, West JL. A whole blood immunoassay using gold nanoshells. Anal Chem. 2003;75:2377–81. doi:10.1021/ac0262210.
8. Mandal D, Maran A, Yaszemski MJ, Bolander ME, Sarkar G. Cellular uptake of gold nanoparticles directly cross-linked with carrier peptides by osteosarcoma cells. J Mater Sci Mater Med. 2009;20(1):347–50. doi:10.1007/s10856-008-3588-x.
9. Ren L, Chow GM. Synthesis of NIR-sensitive Au-$Au_2S$ nanocolloids for drug delivery. Mater Sci Eng C. 2003;23:113–6. doi:10.1016/S0928-4931(02)00247-3.
10. Chow GM, Tan MC, Ren L, Ying JY. NIR-sensitive nanoparticle. US patent application pending.
11. Zhou HS, Honma I, Komiyama H. Controlled synthesis and quantum-size effect in gold-coated nanoparticles. Phys Rev B. 1994;50:12052–6. doi:10.1103/PhysRevB.50.12052.
12. Averitt RD, Sarkar D, Halas NJ. Plasmon resonance shifts of Au-coated $Au_2S$ nanoshells. Phys Rev Lett. 1997;78:4217–20. doi:10.1103/PhysRevLett.78.4217.
13. Tan MC, Ying JY, Chow GM. Structure and microstructure of near infrared-absorbing Au-$Au_2S$ nanoparticles. J Mater Res. 2007;22:2531–8. doi:10.1557/jmr.2007.0314.
14. Tan MC, Ying JY, Chow GM. Composition, particle size, and near-infrared irradiation effects on optical properties of Au-$Au_2S$ nanoparticles. J Mater Res. 2008;23:281–93. doi:10.1557/jmr.2008.0038.
15. Sato S, et al. Nanosecond, high-intensity pulsed laser ablation of myocardium tissue at the ultraviolet, visible, and near-infrared wavelengths: in vitro study. Lasers Surg Med. 2001;29:464–73. doi:10.1002/lsm.10002.
16. Vogel A, Venugopalan V. Mechanisms of pulsed laser ablation of biological tissues. Chem Rev. 2003;103:577–644. doi:10.1021/cr010379n.
17. Waynant RW, Ilev IK, Gannot I. Mid-infrared laser applications in medicine and biology. Philos Trans R Soc Lond A: Math Phys Eng Sci. 2001;359:635–44.
18. Love JC, Estroff LA, Kriebel JK, Nuzzo RG, Whitesides GM. Self-assembled monolayers of thiolates on metals as a form of nanotechnology. Chem Rev. 2005;105:1103–69. doi:10.1021/cr0300789.
19. Caruso F. Nanoengineering of particle surfaces. Adv Mater. 2002;13:11–22. doi:10.1002/1521-4095(200101)13:1<11::AID-ADMA11>3.0.CO;2-N.
20. Ulman A. Formation and structure of self-assembled monolayers. Chem Rev. 1996;96:1533–54. doi:10.1021/cr9502357.
21. Schreiber F. Structure and growth of self-assembling monolayers. Prog Surf Sci. 2000;65:151–256. doi:10.1016/S0079-6816(00)00024-1.
22. Hiemenz PC, Rajagopalan R. Principles of colloid and surface chemistry. New York: Marcel Dekker; 1997.
23. Braun PV. Nanoparticles: spontaneous ligand organization. Nat Mater. 2004;3:281–2. doi:10.1038/nmat1125.
24. Jackson AM, Myerson JW, Stellacci F. Spontaneous assembly of subnanometre-ordered domains in the ligand shell of monolayer-protected nanoparticles. Nat Mater. 2004;3:330–6. doi:10.1038/nmat1116.
25. Wynblatt P, Ku RC. Surface energy and solute strain energy effects in surface segregation. Surf Sci. 1977;65:511–31. doi:10.1016/0039-6028(77)90462-9.
26. Liu F, Metiu H. Dynamics of phase separation of crystal surfaces. Phys Rev B. 1993;48:5808–17. doi:10.1103/PhysRevB.48.5808.
27. U.S. Food and Drug Administration. Toxicological principles for the safety assessment of food ingredients. 2000. http://www.cfsan.fda.gov/~redbook/red-toca.html.
28. Foster KA, Yazdanian M, Audus KL. Microparticulate uptake mechanisms of in vitro cell culture models of the respiratory epithelium. Pharm Pharmacol. 2001;53:57–66.
29. Singh R, et al. Tissue biodistribution and blood clearance rates of intravenously administered carbon nanotube radiotracers. Proc Natl Acad Sci USA. 2006;103:3357–62. doi:10.1073/pnas.0509009103.
30. Ren L, Huang XL, Zhang B, Sun LP, Zhang QQ, Tan MC, et al. Cisplatin-loaded Au-$Au_2S$ nanoparticles for potential cancer therapy: Cytotoxicity, in vitro carcinogenicity, and cellular uptake. J Biomed Mater Res A. 2008;85A:787–96. doi:10.1002/jbm.a.31608.
31. Huang XL, Zhang B, Ren L, Ye SF, Sun LP, Zhang QQ, et al. In vivo toxic studies and biodistribution of near infrared sensitive Au-$Au_2S$ nanoparticles as potential drug delivery carriers. J Mater Sci Mater Med. 2008;19:2581–8. doi:10.1007/s10856-007-3210-7.
32. Kagan VE, Bayir H, Shvedova AA. Nanomedicine and nanotoxicology: Two sides of the same coin. Nanomedicine. 2005;1:313–6.
33. Sayes CM, et al. The differential cytotoxicity of water-soluble fullerenes. Nanolett. 2004;4:1881–7.
34. Kirchner C, et al. Cytotoxicity of colloidal CdSe and CdSe/ZnS nanoparticles. Nanolett. 2005;5:331–8.
35. Yin H, Too HP, Chow GM. The effects of particle size and surface coating on the cytotoxicity of nickel ferrite. Biomaterials. 2005;26:5818–26. doi:10.1016/j.biomaterials.2005.02.036.
36. Licht S. Aqueous solubilities, solubility products and standard oxidation-reduction potentials of the metal sulfides. J Electrochem Soc. 1988;135:2971–5. doi:10.1149/1.2095471.
37. Rabolt JF, Burns FC, Swalen JD. Anisotropic orientation in molecular monolayers by infrared spectroscopy. J Chem Phys. 1983;78:946–52. doi:10.1063/1.444799.
38. Banwell CN, McCash EM. Fundamentals of molecular spectroscopy. 4th ed. London: McGraw-Hill; 2005.
39. Dubois LH, Zegarski BR, Nuzzo RG. Spontaneous organization of carboxylic acid monolayer films in ultrahigh vacuum. Kinetic constraints to assembly via gas-phase adsorption. Langmuir. 1986;2:412–7. doi:10.1021/la00070a006.
40. Calculated using Advanced Chemistry Development (ACD) software, Solaris V4.67 provided by SciFinder Scholar.
41. Kreibig U, Vollmer M. Optical properties of metal clusters. Berlin: Springer; 1995.
42. Linnert T, Mulvaney P, Henglein A. Surface chemistry of colloidal silver: surface plasmon damping by chemisorbed I-, SH-, and $C_6H_5S$-. J Phys Chem. 1993;97:679–82. doi:10.1021/j100105a024.
43. Fox M. Optical properties of solids. New York: Oxford University Press; 2001.

44. Sherman SE, Lippard SJ. Structural aspects of platinum anticancer drug interactions with DNA. Chem Rev. 1987;87:1153–81. doi:10.1021/cr00081a013.
45. Boulikas T, Vougiouka M. Cisplatin and platinum drugs at the molecular level. Oncol Rep. 2003;10:1663–82. Review.
46. Centerwall CR, Goodisman J, Kerwood DJ, Dabrowiak JC. Cisplatin carbonato complexes, Implications for uptake, antitumor properties, and toxicity. J Am Chem Soc. 2005;127:12768–9. doi:10.1021/ja053353c.
47. Berners-Price SJ, Frenkiel TA, Frey U, Ranford JD, Sadler PJ. Hydrolysis products of cisplatin: pKa determinations via [$^{1}$H, 15N] NMR spectroscopy. J Chem Soc Chem Commun. 1992;10: 789–91. doi:10.1039/c39920000789.
48. Bruno TJ, Svoronos PDN. Handbook of basic tables for chemical analysis. 2nd ed. Boca Raton, FL: CRC Press; 2003.
49. Zhang CX, Lippard SJ. New metal complexes as potential therapeutics. Curr Opin Chem Biol. 2003;7:481–9. doi:10.1016/S1367-5931(03)00081-4.
50. Messori L, et al. Gold (III) complexes as potential antitumor agents: Solution chemistry and cytotoxic properties of some selected gold (III) compounds. J Med Chem. 2000;43:3541–8. doi:10.1021/jm990492u.